New Journal of Physics
The open-access journal for physics

# Nanoelectromechanics of suspended carbon nanotubes

**A K Hüttel**[1], **M Poot, B Witkamp and H S J van der Zant**
Molecular Electronics and Devices, Kavli Institute of Nanoscience,
Delft University of Technology, PO Box 5046, 2600 GA Delft, The Netherlands
E-mail: a.k.huettel@tudelft.nl

*New Journal of Physics* **10** (2008) 095003 (13pp)
Received 14 March 2008
Published 30 September 2008
Online at http://www.njp.org/
doi:10.1088/1367-2630/10/9/095003

**Abstract.** We discuss different types of measurements targetting the interplay of mechanical motion with electrical transport in suspended single-wall carbon nanotube devices. In driven resonator experiments, the transversal acoustical vibration mode is detected and identified at room temperature using ac down-mixing techniques. In contrast, low-temperature transport spectroscopy enables the observation of the longitudinal acoustic mode in the quantum limit in single electron tunnelling. This vibrational excitation can also be observed in higher order tunnelling current for appropriate electronic coupling to the leads. Experimental roads towards the quantum limit of the transversal vibration mode—as ultimate quantum-limited beam resonator—are explored, e.g. extending both abovementioned measurement techniques.

**Contents**



[1] Author to whom any correspondence should be addressed.

## 1. Introduction and overview

Research towards observing the quantum limit of mechanical motion has led to a multitude of experimental results in many material systems during recent years [1]–[3]. A promising system for observing the transition between classical mechanics and quantized, nonclassical behaviour is given by single-wall carbon nanotubes (SW-CNTs). SW-CNTs display both extraordinary mechanical and electronic properties. During recent years, research on these macromolecules has covered many areas. This ranges from materials science and industrial applications, focusing mainly on the high tensile strength and Young's modulus [4], to basic research on the nanoelectromechanics of individual nanotubes. Here, they represent the ultimate limit of a mechanical beam resonator, which can be successfully modelled by classical means for suspended nanotubes in the micrometre range [5]. Its exceptionally low mass $\sim 10^{-21}\,\mathrm{kg}\,\mu\mathrm{m}^{-1}$ leads to an oscillator zero-point motion of the transversal mode of over 1 pm, such that direct detection with position-sensing schemes seems feasible. In addition, the entire acoustic and optic phonon spectra [6, 7] predicted for the carbon lattice become relevant, which show a rich variety of modes and cover a wide frequency range. With different measurement techniques, many of these vibrational modes can be resolved.

Figures 1(a) and (b) display a schematic side view and an electron micrograph of a typical nanoelectromechanical SW-CNT device. In a three-terminal arrangement, a suspended single nanotube is clamped between two metallic contact electrodes and suspended above a substrate back-gate. Different measurements on such devices will be discussed further on in this paper. Figure 1(c) sketches the relevant vibrational modes, while figure 1(d) gives an overview of the corresponding energy scales and their dependence on the length $L$ of the suspended nanotube piece.

The radial breathing modes (RBMs) of SW-CNTs, corresponding to optical phonon branches, have found wide attention in optical spectroscopy [6]. Here, e.g. the identification of individual nanotube chirality and tracing of chirality changes at defects has been possible by means of Raman spectroscopy [8]. In addition, the RBMs have been probed in electronic transport by contacting the nanotube with a scanning tunnelling microscope tip [9]. Longitudinal acoustic excitations of SW-CNTs, corresponding to the stretching mode of a bulk beam, can be observed in an energy range around $\sim 1$ meV by low-temperature transport spectroscopy [7]. For both types of vibrational excitations, it is obvious that a quantum mechanical treatment is required, as the quantized nature of the mechanical excitations dominates the behaviour in the measurement.

The transversal acoustic vibration modes of a suspended nanotube, similar to the motion of a guitar or piano string, have a considerably lower energy [5, 6]. Even here, though, the extremely high tensile strength of SW-CNTs with a Young's modulus of typically $E \simeq 1$ TPa [4], combined with the large aspect ratio of nanotube devices, enables the use as radio-frequency mechanical resonators [10]–[12]. Several methods have been utilized for demonstrating lateral mechanical motion of nanotube systems. Approaches to directly observe the motion include real-time visualization as blurring in transmission electron microscopy (TEM) [12, 13] and tracing of the vibration envelope with an atomic force microscope tip [14]. In addition, electronic transport detection of mechanical resonance is possible via signal down-mixing [10, 11], which can also enable the direct identification of the fundamental mode [5, 11].

In the following, we will present the current state of characterizing the transversal acoustic vibrations of suspended SW-CNTs, in analogy to conventional NEMS and MEMS beam

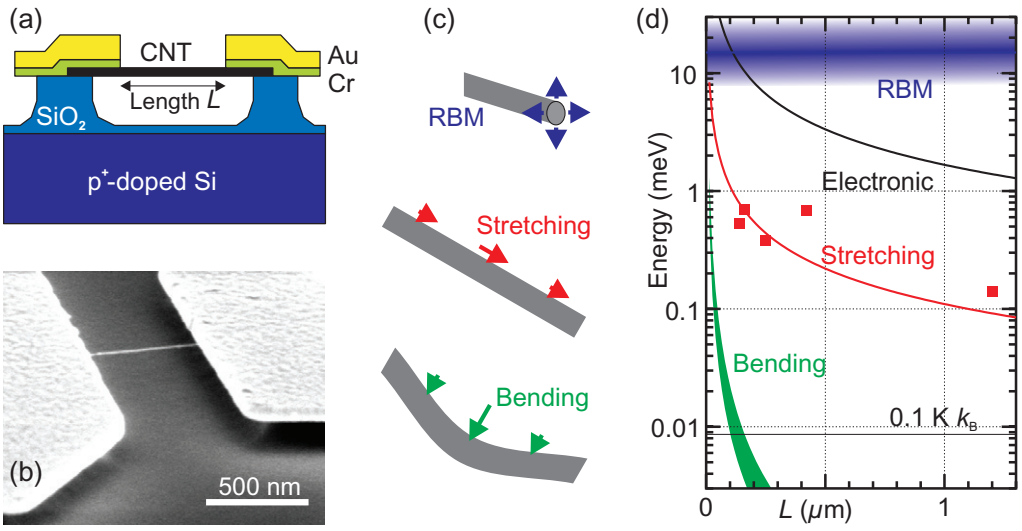


**Figure 1.** (a) Side-view sketch of the geometry of a typical three-terminal nanoelectromechanical suspended single carbon nanotube device. The nanotube stretches freely between metallic contact electrodes. (b) Corresponding scanning electron micrograph. (c) Schematic drawing of the vibrational modes and (d) predicted corresponding oscillator energy scales $\hbar\omega$ of suspended nanotube segments, taking into account the characteristic material properties of SW-CNTs. The radial breathing mode (RBM) scales with $1/d$ ($d$ being the nanotube diameter), and the transversal 'bending' mode is both diameter and tension dependent. Thus, both are characterized by a frequency range (indicated in the figure by a widening of the green and blue lines). Data points indicate observations of harmonic excitation spectra, i.e. quantized vibration modes, in low-energy transport spectroscopy experiments (see section 3).

resonators, in driven oscillator experiments. The longitudinal acoustic vibrations, in contrast, are shown to be visible in the quantum limit in both first-order and higher order tunnelling in low-temperature transport spectroscopy. Finally, we discuss possible ways of approaching the quantum limit for the transversal vibration as well.

## 2. Electrostatically driven nanotube resonators

In the field of nanomechanics, suspended carbon nanotube resonators form the ultimate size limit of a mechanical beam resonator [10, 11, 14, 15]. Due to the relatively large resistance of nanotubes of at least several kiloohms, magnetomotive driving and detection of the mechanical resonator cannot be used. Thus, in room-temperature experiments, frequency mixing techniques are employed for down-mixing the ac conductance and detecting mechanical capacitance changes. The nanotube resonator is driven electrostatically by applying both ac and dc voltages, $V_g^{ac}$ and $V_g^{dc}$, respectively, to an underlying back-gate electrode formed by the wafer substrate (as sketched in figure 1(a)). The interaction capacitance between resonator and back-gate electrode can be written as the sum of a static, time-independent term $C_g^{dc}$ corresponding to the time-averaged position of the nanotube, and a contribution $C_g^{ac}(t)$ oscillating at the frequency of

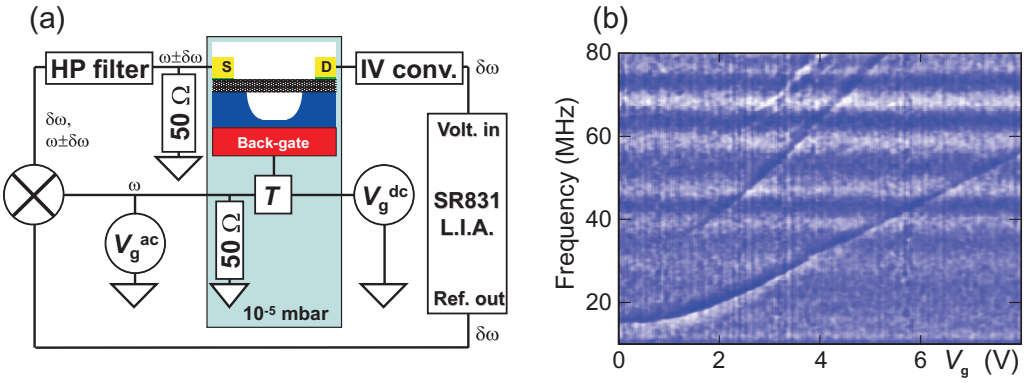


**Figure 2.** (a) Schematic overview of the measurement setup used for detecting vibrational resonances of suspended carbon nanotubes via frequency down-mixing [11]. While the nanotube resonator is driven at frequency $\omega$, a source–drain bias at $\omega \pm \delta\omega$ is applied; the gate-dependence of the nanotube conductance enables effective read-out of the mechanical response at the difference frequency $\delta\omega$. (b) Measured current at frequency $\delta\omega$ in a $L = 1\,\mu$m nanotube device, displaying several gate-voltage-dependent mechanical resonance features. To emphasize the mechanical resonances, a high pass filter was used for removing the slow varying electrical background signal. Due to slack in the nanotube, multiple vibration modes are visible.

the mechanical motion, i.e.

$$C_g(t) = C_g^{dc} + C_g^{ac}(t). \tag{1}$$

When the ac driving voltage frequency nears the frequency of one of the mechanical eigenmodes, the oscillatory nanotube displacement increases thereby modulating the distance between the back-gate and the nanotube. This leads to an increase in the value of $C_g^{ac}(t)$ superimposed on the static capacitance $C_g^{dc}$ between the nanotube and the back-gate. For semiconducting nanotubes at room temperature, it is well known that the conductance of the nanotubes depends on the charge induced on the tube. The ac displacement of the resonator near a mechanical resonance hence also induces charge $Q^{ac}(t) = C_g^{ac}(t)V_g$ and thus changes the conductance through the ac capacitance:

$$G^{ac} = \frac{dG}{dV_g}\left(V_g^{ac} + V_g^{dc}\frac{C_g^{ac}}{C_g^{dc}}\right), \tag{2}$$

where the factor $\frac{dG}{dV_g}$ denotes the transconductance of the device. This transconductance typically depends on the dc gate-voltage for semiconducting nanotubes, and is in our devices of the order 1–10 $\mu$S V$^{-1}$. By applying an ac source–drain bias $V_{sd}^{ac}$ with a small frequency offset $\delta\omega$, the ac conductance is mixed with the ac bias voltage, resulting in a low-frequency current $\bar{I} \propto V_{sd}^{ac} G^{ac}$, which is modulated at the difference frequency and can be extracted by means of a lock-in amplifier [10, 11]. The setup of this measurement is sketched in figure 2(a).

Unlike common top-down NEMS resonators, due to the small cross-sectional areas of SWCNTs, tension plays an important role for the transversal vibration mode. Calculations show that tension can be used as an instrument for tuning the mechanical resonance frequencies [16].

This has been confirmed by experiments [10, 11], which show that the mechanical resonance frequencies are easily increased up to 200% of their zero-tension value. Sazonova *et al* [10] have observed multiple gate-tunable resonances at specific driving frequencies in the down-mixed current flowing through the nanotube when the dc gate-voltage (and through it the tension) was increased. These multiple resonances can be attributed to several in-plane and out-of-plane flexural modes of a slack suspended nanotube (hanging chain) [17]. Here, the nanotube itself is longer than the distance between its clamping points. Witkamp *et al* [11] measured a single gate-tunable resonance in several devices and identified it as the fundamental bending mode vibration of a nanotube that is under small compressive tension, but not buckled. A common feature in these devices (both for slack tubes and for nanotubes under tension) is that the quality factors of the mechanical resonances are at room temperature rather low, i.e. on the order of a few hundred.

Higher mechanical eigenfrequencies can be reached by either using shorter nanotube resonators—which increases the fundamental bending mode frequencies—or by using tension to increase the mechanical resonance frequencies to a much higher value. Both methods decrease, however, the amplitude of the resonator, and thereby the detected ac current signal [5]. Currently, the high frequency limit of the described measurement technique is given by a few hundred MHz, corresponding to a vibrational quantum energy of $\hbar\omega \sim 1\,\mu$eV. At these frequencies, the mechanical resonance peaks are hard to distinguish from background fluctuations of the conductance and therefore become increasingly more difficult to observe. Note that in our setup the mentioned background fluctuations do not form the intrinsic limitation of detection sensitivity. This limit is given by the thermal fluctuations of the nanotube position. The origin of the background fluctuations is not understood; one possibility may be the motion of charges in the oxide layer.

## 3. Quantized mechanical motion of the longitudinal acoustic mode

When suspended nanotube devices, as discussed in the previous section, are cooled down to cryogenic temperatures, tunnel barriers between the metallic leads and the nanotube may lead to the formation of a quantum dot within the nanotube [21, 22]. The gate dependence of the conductance can display different behaviour, depending on the coupling between the nanotube and the leads. For large couplings $\Gamma$, Fabry–Perot behaviour with a slowly varying conductance is expected [23], whereas for small $\Gamma$, Coulomb blockade (CB) is observed [21, 22, 24, 25]. In the latter case, the conductance consists of a series of sharp peaks with a width depending on $\Gamma$ and the electron temperature. Figure 3(a) shows a sketch of such a suspended nanotube quantum dot, with the highly doped wafer substrate acting as back-gate electrode. Since suspending the device is done by isotropic etching with buffered hydrofluoric acid, the contact electrodes are also partially underetched.

In the parameter regime dominated by CB physics, the quantum mechanical level spectrum of the confined electronic system can be characterized by transport measurements [18]. By recording in the so-called stability diagram—as drawn in figure 3(b)—the differential conductance $\mathrm{d}I/\mathrm{d}V_{\mathrm{sd}}$ as a function of gate voltage $V_{\mathrm{g}}$ and source–drain voltage $V_{\mathrm{sd}}$, both semiconducting and metallic nanotubes have been characterized in literature, leading to striking agreements between the theory and observations [26]–[28]. An important property of suspended nanotube systems is that in the quantum limit of the mechanical mode, i.e. for $\hbar\omega > k_{\mathrm{B}}T$, due to the Franck–Condon effect mechanical modes also become visible in transport [7, 20]. In short,

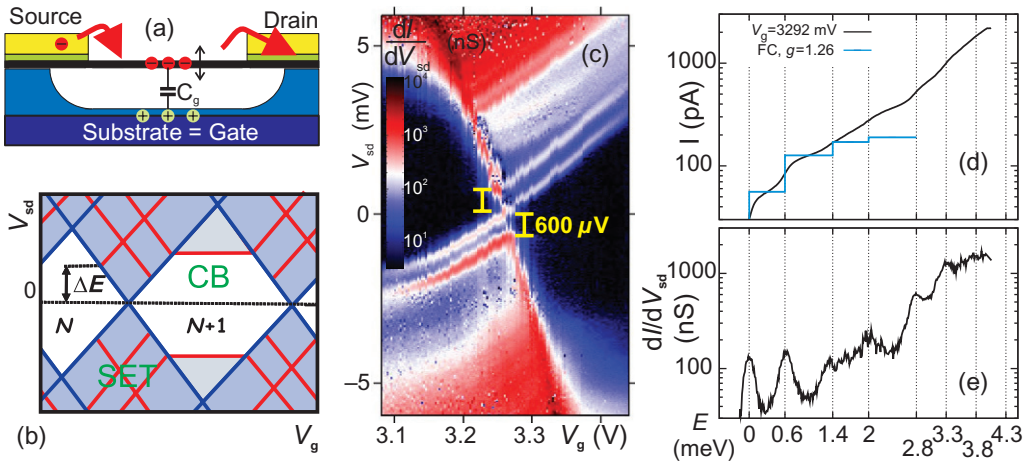


**Figure 3.** (a) Schematic drawing of a suspended carbon nanotube as a single electron tunnelling (SET) device. Due to the choice of chromium/gold contacts, tunnel barriers defining a quantum dot are formed at the nanotube–contact electrode interface. (b) Basic principles of transport spectroscopy [18]. Differential conductance $\mathrm{d}I/\mathrm{d}V_{\mathrm{sd}}$ is measured as a function of gate voltage $V_{\mathrm{g}}$ and source–drain voltage $V_{\mathrm{sd}}$, resulting in the characteristic pattern of diamond-shaped regions of CB. In the regions of SET, changes in tunnel rates occur whenever an additional transport channel becomes energetically possible. Higher order processes may lead to structures within the CB regions [19]. (c) Example measurement of the differential conductance $\mathrm{d}I/\mathrm{d}V_{\mathrm{sd}}$ of a suspended SW-CNT quantum dot, displaying a large number of excitations in the low-energy spectrum (see text). Figures (d) and (e) display traces $I(V_{\mathrm{sd}})$ and $\mathrm{d}I/\mathrm{d}V_{\mathrm{sd}}(V_{\mathrm{sd}})$, respectively, from (c) at $V_{\mathrm{g}} = 3292\,\mathrm{mV}$. The $x$-axis has been rescaled to reflect the excitation energies that the differential conductance maxima correspond to (see text). The blue line represents the calculated zero-temperature current steps of a Franck–Condon model with strong relaxation and electron–phonon coupling $g = 1.26$ [20].

electrostatic coupling between the gate electrode and the suspended nanomechanical system leads to a dependence of the position of the mechanical oscillator ground state on the number of trapped charges. The vibrational wavefunction overlap of the $N$ and $N+1$ charge carrier states required for SET is thus reduced by the so-called Franck–Condon factors. At finite source–drain voltage $V_{\mathrm{sd}}$, whenever an additional vibrational quantum is encompassed by the energy window, this reduction is partially lifted, leading to steps in tunnel current equidistant in $V_{\mathrm{sd}}$. The entire nanotube acts as a quantized single nanomechanical oscillator. The coupling strength between the electronic and the mechanical systems can be characterized by a dimensionless parameter $g = \frac{1}{2}(x/x_0)^2$, where $x$ is the shift of the ground-state position induced by adding one elementary charge, and $x_0$ describes the zero-point motion of the mechanical oscillator. In the simplest case, the Franck–Condon model assumes fast relaxation of the mechanical system to its ground state (compared with the electronic tunnel rates), but different scenarios may be envisaged [29].

The energy resolution of transport spectroscopy measurements is limited by several factors, including the electron temperature, the natural linewidth of the involved quantum states, and fluctuations of the electrode potentials. To date, a typical SW-CNT device has a length of $100\,\mathrm{nm} \leqslant L \leqslant 1\,\mu\mathrm{m}$, which excludes the bending mode from direct observation (see figure 1(d)). Data on harmonic excitation spectra observed in transport, however, support a considerable electron–vibration coupling of $g \sim 1$ for the longitudinal acoustic vibration mode [7]. The data points in figure 1(d) provide an overview of the energy scale determined from harmonic spectra observed so far, extending the results of [7] with new measurements.

Figure 3(c) displays an example transport spectrum of a 160 nm long suspended carbon nanotube. The data have been recorded at an electron temperature of $T_{\mathrm{el}} \simeq 100\,\mathrm{mK}$ and a cryostat temperature of $T \simeq 20\,\mathrm{mK}$ in a $^3\mathrm{He}/^4\mathrm{He}$ dilution refrigerator. For this device length, a stretching mode energy of $\hbar\omega = 0.7\,\mathrm{meV}$ is predicted. In the plot of figure 3(c), a dominant energy scale of 0.6 meV is observed, in reasonable agreement with this prediction. Figure 3(d) and (e) display data traces of current and differential conductance, respectively, for the constant $V_{\mathrm{g}} = 3292\,\mathrm{mV}$. From the slopes of the edges of the CB region in the stability diagram of figure 3(c), one can obtain the capacitance ratios between gate, source and drain electrodes and the quantum dot, and thereby the conversion factors relating the applied voltages to the local electrostatic potential. This has been used for re-scaling the $x$-axis to reflect the excitation energies that the current steps correspond to. Assuming fast vibrational relaxation, from the first two current steps in figure 3(d), a value of $g \simeq 1.3$ can be estimated [20]. The blue line in figure 3(d) indicates the current step heights predicted by such a Franck–Condon model. This result, similar to previous measurements [7], suggests strong electron–vibron interaction.

In detail, however, the spectrum of figures 3(c)–(e) is not given by equidistant excitations, but by pairs of excitations—a fundamental line is accompanied by a parallel excitation at $\sim$0.6 meV higher energy. The second one of these line pairs displays a considerable gate voltage or bias dependence of excitation energy. Similar 'dressing' of excitations by vibrational modes has been described by extensions of the Franck–Condon model, taking into account additional electronic degrees of freedom or modification of the vibration frequency at a change of the number of trapped charge carriers [30, 31].

Figure 4(a) displays the transport spectrum of the same device as in figure 3(c) for more negative gate voltage $V_{\mathrm{g}}$. Here, while CB still dominates transport, a considerably stronger coupling between the quantum dot and leads is observed. Such a change of electronic coupling with gate voltage $V_{\mathrm{g}}$ is commonly observed in carbon nanotubes. The higher coupling leads to larger currents, peak broadening and higher order tunnelling processes in the CB region [19]. A striking feature of the data is a multitude of strongly gate-dependent inelastic co-tunnelling resonances. For comparison, the scale $\Delta E = 0.6\,\mathrm{mV}$ obtained in figure 3(c) has been indicated. It nearly coincides in many places with the energetic distance of the co-tunnel resonances; a direct read-out of the bias distance between the adjacent lines here results in a slightly higher value. The co-tunnel resonances persist upto a temperature of over 0.5 K, as can be seen from the traces $\mathrm{d}I/\mathrm{d}V_{\mathrm{sd}}(V_{\mathrm{sd}})$ shown in figure 4(b). Note that the co-tunnel features appear as peaks instead of steps. This may hint at non-equilibrium effects or Kondo interactions.

Although mechanisms for gate-dependent co-tunnel resonances have very recently been proposed and identified in literature for SW-CNT quantum dots [32], explaining the gate dependence of inelastic co-tunnelling as observed here has not been possible so far. The same is true for the 'dressing' effect observed in figures 3(c)–(e). The obvious recurrence of the characteristic energy scale of the longitudinal acoustic vibration mode strongly suggests

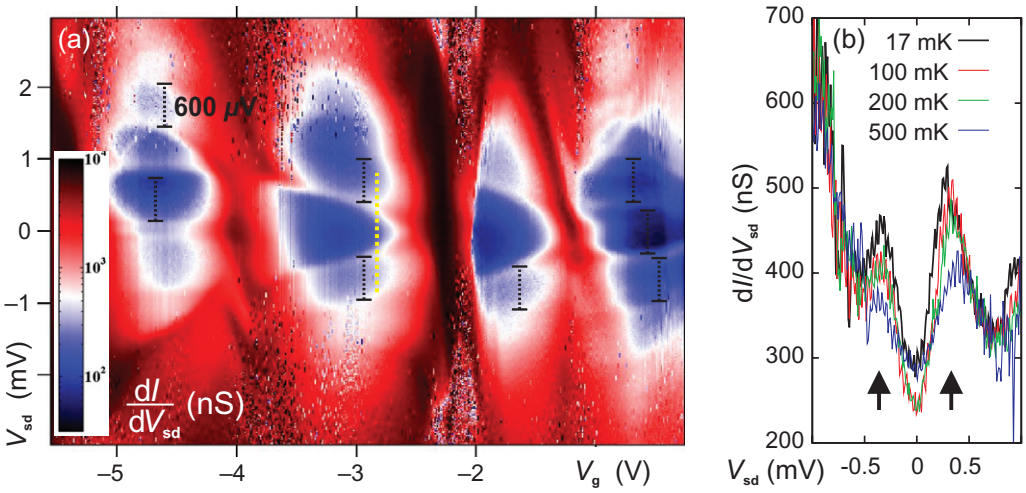


**Figure 4.** (a) Differential conductance of the same device also shown in figure 3(c), but for a different gate voltage region displaying a larger dot–leads coupling. While CB still dominates transport, a large number of strongly gate-dependent inelastic co-tunnelling resonances is observed, with a characteristic energy scale close to the 0.6 meV in figure 3(c). (b) Temperature dependence of one exemplary co-tunnel step, taken at $V_g = -2.84$ V as indicated by a yellow dotted line in (a).

a common mechanical effect in both cases. Mechanisms of interaction between, e.g., co-tunnelling or the Kondo effect and vibrational modes remain an area of active theoretical research to date.

## 4. Outlook—Bending-mode spectroscopy and the quantum limit

The transition towards quantized mechanical motion for the transversal vibration mode may provide a nanoelectromechanical system that can exist as both conventional mechanical beam resonator and quantized oscillator, one of the main goals of NEMS research. Fundamentally different ways towards observing quantum mechanical effects related to the transversal or bending vibration mode are possible. We will briefly comment on three such approaches.

### *4.1. Driven-motion detection and Coulomb blockade*

As a first step, one may consider extending the beam resonator detection scheme of section 2 to the low-temperature limit. However, as explained in section 3, different situations can occur when cooling a nanotube to cryogenic temperatures. When the coupling to the leads is large enough, the conductance varies only slowly with gate voltage and the mixing technique can be used for detecting the motion of the nanotube. However, at small coupling $\Gamma$, CB occurs, and a series of discrete peaks is visible in the gate-dependence of the conductance. Due to the sharpness of these peaks ($\ll V_g^{ac}$), the usual derivation of the mixing current breaks down, and one may ask whether it is possible to measure the driven vibrations of the nanotube at all with the frequency down-mixing technique.

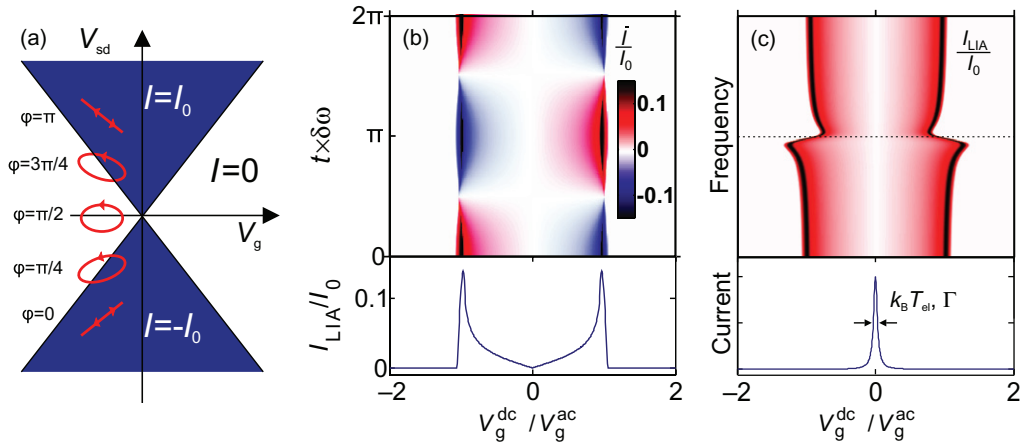


**Figure 5.** (a) Schematic of the effect of ac gate and bias voltages in the stability diagram of a quantum dot, where in the SET regime a single transport channel carries a current $\pm I_0$. Ellipsoidal trajectories through the diagram are traced, with a shape depending on the phase difference $\varphi$ between the two ac voltages. (b) Calculated time dependence (top) of the average current $\bar{I}$ (in units of $I_0$) for $V_{sd}^{dc} = 0$, $\varphi = 0$ and finite $V_g^{ac}$, when modulating the source–drain voltage with $V_{sd}^{ac} = 0.1 \cdot \cos(\delta\omega t)$. The bottom panel shows the component $I_{LIA}$ of $\bar{I}$ at the lock-in frequency $\delta\omega$. (c) Simulated down-mixed nanotube current $I_{LIA}$ (top panel) when sweeping the driving frequency around the mechanical eigenfrequency (dashed line) for the same conditions as (b). The sharpness of the edge of the signal determines how easily the resonance can be observed. In practice, this may be limited by the width of the Coulomb peak on which the signal is mixed (bottom panel), i.e. by the temperature $k_B T$ or coupling $\Gamma$.

To analyse mixing in the presence of CB, a simple model is used, where tunnelling between the nanotube and the leads takes place through a single quantum level. The current in the blocked regions is zero, while in the conducting regions it assumes a constant value $\pm I_0$. This can be written as $I = I_0 \cdot [H(V_g + V_{sd}/2) - H(V_g - V_{sd}/2)]$, where $H$ is the Heaviside stepfunction; such a current dependence on $V_g$ and $V_{sd}$ is depicted in figure 5(a), sketching the stability diagram of the quantum dot.

When using the mixing technique, the bias and gate voltages $V_{sd}$ and $V_g$ are the sum of ac and dc components. In other words, while time elapses, the bias and gate voltages trace trajectories through the stability diagram. This is sketched in figure 5(a), depending on the phase relationship between $V_g^{ac}$ and $V_{sd}^{ac}$. The trajectories are ellipsoidal since $V_g^{ac}$ and $V_{sd}^{ac}$ vary as $\cos\omega t$ and $\cos(\omega t + \varphi)$. Well inside the CB region, the current remains zero at all times. However, when such a trajectory crosses the edge of the CB region, fast current oscillations occur, since the quantum dot within the nanotube is continuously switching into and out of the blockade. In the experiment, only the low-frequency components of the current are measured. Thus, we calculate the corresponding time-averaged signal $\bar{I}$, obtaining

$$\bar{I} = I_0 \cdot A(V_-^{dc}/V_-^{ac}) - I_0 \cdot A(V_+^{dc}/V_+^{ac}), \tag{3}$$

with the function $A$ defined as

$$A(v) = \begin{cases} 0 & v \geqslant 1 \\ \arccos(v)/\pi & -1 \leqslant v \leqslant 1, \\ 1 & v \leqslant -1, \end{cases} \tag{4}$$

and

$$V_{\pm}^{\mathrm{ac}} = \left((V_{\mathrm{g}}^{\mathrm{ac}})^2 + (V_{\mathrm{sd}}^{\mathrm{ac}}/2)^2 \pm V_{\mathrm{g}}^{\mathrm{ac}} V_{\mathrm{sd}}^{\mathrm{ac}} \cos(\varphi)\right)^{1/2}, \tag{5}$$

$$V_{\pm}^{\mathrm{dc}} = V_{\mathrm{g}}^{\mathrm{dc}} \pm V_{\mathrm{sd}}^{\mathrm{dc}}/2. \tag{6}$$

The signal depends on the position in the stability diagram via $V_{\mathrm{g}}^{\mathrm{dc}}$ and $V_{\mathrm{sd}}^{\mathrm{dc}}$, on the magnitudes of the ac gate and source–drain voltages $V_{\mathrm{g}}^{\mathrm{ac}}$ and $V_{\mathrm{sd}}^{\mathrm{ac}}$, and on the phase difference $\varphi$ between them.

In an experimental realization, the frequencies of the two ac signals differ. Details depend on the exact setup used: with the two-generator technique [10], because of the small frequency offset the phase difference is effectively time dependent, i.e. $\varphi = \varphi_0 + \delta\omega t$, whereas in our one-generator setup (figure 2) the source–drain ac voltage is amplitude-modulated, i.e. $V_{\mathrm{sd}}^{\mathrm{ac}} \to V_{\mathrm{sd}}^{\mathrm{ac}} \cos(\delta\omega t)$. In both cases, the time-averaged current contains low-frequency oscillations at the offset frequency $\delta\omega$ that can be measured using a lock-in amplifier. In the following analysis, only the single-generator setup is studied in detail.

The time-averaged current $\bar{I}$ is calculated numerically while modulating $V_{\mathrm{sd}}^{\mathrm{ac}}$. From this, the component of $\bar{I}$ at the offset frequency $\delta\omega$ is extracted, resulting in the signal plotted in the lower panel of figure 5(b) that a lock-in amplifier would detect. One sees that the Coulomb peak is widened due to the ac voltages, but it still contains a sharp transition between the regions with and without current. Note that this background signal is always present, even without any displacement of the nanotube. The effect of nanotube vibrations is an apparent change in the magnitude and phase of the ac gate voltage when $C_{\mathrm{g}}^{\mathrm{ac}} \neq 0$, as can be seen from equation (2). The effects of this feature become clear when the down-mixed current is calculated for different driving frequencies (figure 5(c), top panel). Off-resonance, the original background signal from the bottom panel of figure 5(b) is obtained. When approaching the mechanical eigenfrequency (dashed line in figure 5(c)) a clear resonance can be seen, which is best visible in the shape of the signal. This stands in contrast to the usual mixing signal (see section 2), where the resonance appears in the magnitude of the current.

The sharp edges of the widened Coulomb peak (see the lower panel of figure 5(b)) enable sensitive detection of vibrational motion of the nanotube. Its finite outer slope (i.e. towards higher absolute values of $V_{\mathrm{g}}^{\mathrm{dc}}/V_{\mathrm{g}}^{\mathrm{ac}}$) is due to the nonzero value of $V_{\mathrm{sd}}^{\mathrm{ac}}$. A reduction of this voltage gives an even sharper peak and therefore a higher sensitivity. However, at some point, the broadening of the original Coulomb peak (lower panel of figure 5(c)) due to the electron temperature or to coupling to the leads starts to dominate this slope and the sensitivity can no longer be increased by reducing $V_{\mathrm{sd}}^{\mathrm{ac}}$.

In conclusion, it is possible to detect the motion of a vibrating nanotube in the CB regime using frequency down-mixing. However, a more detailed analysis is needed for finding the ultimate limit on the sensitivity of this method.

### *4.2. Zero-point motion detection*

The objective of observing a mechanical resonator in its quantum mechanical ground state excludes applying a driving signal. Thus, a mesoscopic position detector needs to be coupled

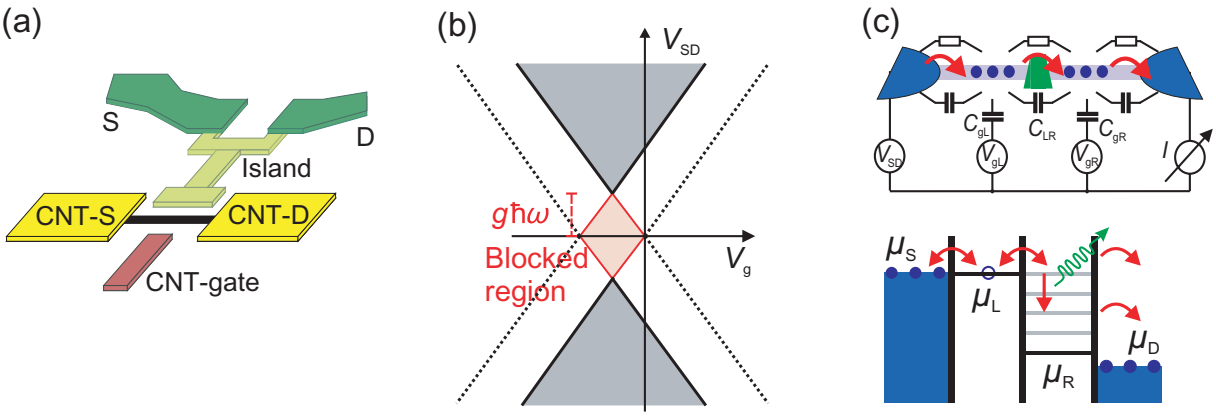


**Figure 6.** (a) Schematic drawing of a device geometry coupling a single electron transistor as charge detector with a suspended carbon nanotube quantum dot. For simplicity, additional control gates of the transistor are omitted; for dimensions, see the main text. (b) Prediction of 'classical' current blockade through an oscillating quantum dot (adapted from [33]): in the case analogous to very strong electron–vibron coupling $g$, current may be blockaded for $|eV_{sd}| \leqslant g\hbar\omega$ even if $\hbar\omega < k_B T < g\hbar\omega$. (c) Using a double quantum dot as phonon spectrometer [34]: circuit diagram and energy level scheme for the limiting case of weak interdot coupling.

to the mechanical system. This leads the way to many different types of experiments, from the detection of the mechanical zero point fluctuation by, e.g., measuring the displacement noise as a function of device temperature, to detector backaction effects and finally to the implementation of a fully coherent quantum–mechanical coupling between the mechanical resonator and nearby detector quantum systems (or 'qubits'). Several detection and thereby coupling schemes have been proposed for mesoscopic resonators. One possibility is the use of charge sensing by means of a nearby metallic single electron transistor [2].

A simplified example of an integrated single electron transistor–suspended CNT device geometry is sketched in figure 6(a). The transistor island is extended as a capacitive 'antenna', maximizing the interaction. In the following, we will provide a rough estimate of the possible deflection sensitivity. The minimal distance to the nanotube is given by fabrication (alignment) precision. For a nanotube resonator with length $L = 250\,\mathrm{nm}$, diameter $d = 1.4\,\mathrm{nm}$, and distance to the antenna $h = 75\,\mathrm{nm}$, an interaction capacitance of $C_i \simeq 2\,\mathrm{aF}$ can be calculated. Approximating the deflection sensitivity with the derivative of $C_i$ by the nanotube–antenna distance $h$, one obtains $\partial C_i/\partial h \simeq 0.005\,\mathrm{zF\,pm^{-1}}$. Assuming a typical value for the charging energy of a nanotube quantum dot of $E_C = 4\,\mathrm{meV}$ [27] and a charge of $Q = 100\,e^-$ on the nanotube, this results in an influenced charge per nanotube deflection of $q \simeq 1 \times 10^{-5}\,e^-\,\mathrm{pm^{-1}}$ on the transistor island. As a reference, the characteristic length associated with the zero-point motion of the mechanical oscillator is $x_0 = \sqrt{\hbar/m\omega} \simeq 10\,\mathrm{pm}$.

The current state of the art in terms of charge-detection noise, as published in [2], is given by $S_Q \simeq 8 \times 10^{-6}\,e^-\,\sqrt{\mathrm{Hz}^{-1}}$. However, published data on room-temperature measurements indicate low mechanical quality factors [10, 11]. One can conclude that even though the resonator properties may improve at cryogenic temperatures, for resonator frequencies of the

order ∼1 GHz, the requirement of a sufficient signal-to-noise ratio still provides a considerable challenge.

### *4.3. Energy spectroscopy of the bending mode*

By optimizing nanotube devices towards shorter suspended length, bending mode frequencies in the GHz range can be obtained (cf figure 1(c)); around a length of $L = 50$ nm, detection of the bending mode in transport spectroscopy seems feasible. For the bending mode, electrostatic modelling predicts a larger electron–vibron coupling $g$ than for the stretching mode, because the mechanical motion can be parallel to the electrical field lines (i.e. towards the gate electrode). Estimates, however, show that $g$ decreases for shorter devices due to the smaller beam deflection. In addition, it strongly depends on the gate voltage $V_g$ via the trapped charge and the tension in the nanotube.

In order to reach high mechanical resonance frequencies, we have recently started performing spectroscopic measurements on nanotube segments down to a length of $L = 65$ nm. Experiments have not revealed any low-energy structure as yet. In view of the large number of parameters influencing both the spectroscopic resolution and the bending mode frequency—e.g. the quantum dot–lead coupling $\Gamma$, the tension of the nanotube induced during fabrication, or the nanotube diameter $d$—the observation of the lateral oscillator quantization may well be just one small step away.

The magnitude of the electron–vibron coupling involved can also be verified for longer nanotube resonator segments by looking at the classical counterpart of Franck–Condon blockade. Calculations by Pistolesi and Labarthe [33] show that here a large coupling between electronic and mechanical systems (corresponding to $g \gg 1$) leads to a suppression of low-bias current in an energy region corresponding to $e|V_{sd}| < g\hbar\omega$ independent of gate voltage $V_g$, even though the temperature is not sufficiently low for resolving the vibrational quantization and the quantum limit is thus not reached. This is illustrated in figure 6(b) with a schematic stability diagram.

Finally, increasing the experimentally available spectroscopic resolution can be done by defining double quantum dots [34]–[38]—with one quantum dot freely suspended—within the nanotube. Choosing a very weak coupling of the quantum dot states to the leads and each other, a highly sensitive phonon spectrometer may be formed [39]. The definition of a (partially) suspended double quantum dot, however, requires a significantly more complex chip fabrication due to the requirement of both a central barrier gate electrode and localized etching [34].

## Acknowledgments

We thank Maarten Wegewijs, Yaroslav Blanter and Ivar Martin for insightful discussions, and Bert Otte and Hari Pathangi for experimental help. Financial support by the Dutch organization for Fundamental Research on Matter (FOM), the NWO VICI program and NanoNed is acknowledged.

## References

[1] Blencowe M 2004 *Phys. Rep.* **395** 159
[2] Naik A, Buu O, LaHaye M D, Armour A D, Clerk A A, Blencowe M P and Schwab K C 2006 *Nature* **443** 193

[3] Corbitt T, Wipf C, Bodiya T, Ottaway D, Sigg D, Smith N, Whitcomb S and Mavalvala N 2007 *Phys. Rev. Lett.* **99** 160801
[4] Yu M F, Files B S, Arepalli S and Ruoff R S 2000 *Phys. Rev. Lett.* **84** 5552
[5] Poot M, Witkamp B, Otte M A and van der Zant H S J 2007 *Phys. Status Solidi* b **244** 4252
[6] Dresselhaus M S and Eklund P C 2000 *Adv. Phys.* **49** 705
[7] Sapmaz S, Jarillo-Herrero P, Blanter Y M, Dekker C and van der Zant H S J 2006 *Phys. Rev. Lett.* **96** 026801
[8] Anderson N, Hartschuh A and Novotny L 2007 *Nano Lett.* **7** 577
[9] LeRoy B J, Lemay S G, Kong J and Dekker C 2004 *Nature* **432** 371
[10] Sazonova V, Yaish Y, Ustunel H, Roundy D, Arias T A and McEuen P L 2004 *Nature* **431** 284
[11] Witkamp B, Poot M and van der Zant H 2006 *Nano Lett.* **6** 2904
[12] Jensen K, Weldon J, Garcia H and Zettl A 2007 *Nano Lett.* **7** 3508
[13] Babic B, Furer J, Sahoo S, Farhangfar S and Schonenberger C 2003 *Nano Lett.* **3** 1577
[14] Garcia-Sanchez D, Paulo A S, Esplandiu M J, Perez-Murano F, Forro L, Aguasca A and Bachtold A 2007 *Phys. Rev. Lett.* **99** 085501
[15] Peng H B, Chang C W, Aloni S, Yuzvinsky T D and Zettl A 2006 *Phys. Rev. Lett.* **97** 087203
[16] Sapmaz S, Blanter Y M, Gurevich L and van der Zant H S J 2003 *Phys. Rev.* B **67** 235414
[17] Üstünel H, Roundy D and Arias T A 2005 *Nano Lett.* **5** 523
[18] Kouwenhoven L P, Marcus C M, McEuen P L, Tarucha S, Westervelt R M and Wingreen N S 1997 *Mesoscopic Electron Transport* ed L L Sohn, L P Kouwenhoven and G Schön (Dordrecht: Kluwer)
[19] De Franceschi S, Sasaki S, Elzerman J M, van der Wiel W G, Tarucha S and Kouwenhoven L P 2001 *Phys. Rev. Lett.* **86** 878
[20] Braig S and Flensberg K 2003 *Phys. Rev.* B **68** 205324
[21] Bockrath M, Cobden D H, McEuen P L, Chopra N G, Zettl A, Thess A and Smalley R E 1997 *Science* **275** 1922
[22] Tans S J, Devoret M H, Dai H, Thess A, Smalley R E, Geerligs L J and Dekker C 1997 *Nature* **386** 474
[23] Liang W, Bockrath M, Bozovic D, Hafner J H, Tinkham M and Park H 2001 *Nature* **411** 665
[24] Kulik I O and Shekhter R I 1975 *Sov. Phys.—JETP* **41** 308
[25] Averin D V and Likharev K K 1986 *J. Low Temp. Phys.* **62** 345
[26] Jarillo-Herrero P, Sapmaz S, Dekker C, Kouwenhoven L P and van der Zant H S J 2004 *Nature* **429** 389
[27] Sapmaz S, Jarillo-Herrero P, Kong J, Dekker C, Kouwenhoven L P and van der Zant H S J 2005 *Phys. Rev.* B **71** 153402
[28] Oreg Y, Byczuk K and Halperin B I 2000 *Phys. Rev. Lett.* **85** 365
[29] Mitra A, Aleiner I and Millis A J 2004 *Phys. Rev.* B **69** 245302
[30] Nowack K C and Wegewijs M R 2005 Vibration-assisted tunneling through competing molecular states *Preprint* cond-mat/0506552
[31] Wegewijs M R and Nowack K C 2005 *New J. Phys.* **7** 239
[32] Holm J V, Jorgensen H I, Grove-Rasmussen K, Paaske J, Flensberg K and Lindelof P E 2008 *Phys. Rev.* B **77** 161406
[33] Pistolesi F and Labarthe S 2007 *Phys. Rev.* B **76** 165317
[34] Hüttel A K, Witkamp B and van der Zant H S J 2007 *Phys. Status Solidi* b **244** 4184
[35] van der Wiel W G, Franceschi S D, Elzerman J M, Fujisawa T, Tarucha S and Kouwenhoven L P 2003 *Rev. Mod. Phys.* **75** 1
[36] Mason N, Biercuk M J and Marcus C M 2004 *Science* **303** 655
[37] Sapmaz S, Meyer C, Beliczynski P, Jarillo-Herrero P and Kouwenhoven L 2006 *Nano Lett.* **6** 1350
[38] Gräber M R, Weiss M, Oberholzer S and Schönenberger C 2006 *Semicond. Sci. Technol.* **21** S64
[39] Fujisawa T, Oosterkamp T H, van der Wiel W G, Broer B W, Aguado R, Tarucha S and Kouwenhoven L P 1998 *Science* **282** 932